Meteorology

Sensitivity analysis of atmospheric phenomena models for precipitation assessment on the Paraíba do Sul River watershed

Análise de sensibilidade de modelos de fenômenos atmosféricos para avaliar precipitação na bacia hidrográfica do Rio Paraíba do Sul

Dhiego da Silva Sales[I] (iD)**, Jader Lugon Junior[I,II]** (iD)**,
Vicente de Paulo Santos de Oliveira[I,II]** (iD)**, Nivaldo Silveira Ferreira[III]** (iD)**,
Antonio Silva Neto[IV]** (iD)

[I] Instituto Federal de Educação, Ciência e Tecnologia Fluminense, Macaé, RJ, Brazil
[II] Instituto Federal de Educação, Ciência e Tecnologia Fluminense, Campos dos Goytacazes, RJ, Brazil
[III] Universidade Estadual Norte Fluminense, Macaé/RJ, Brazil
[IV] Universidade do Estado do Rio de Janeiro, Instituto Politécnico, Nova Friburgo, RJ, Brazil

ABSTRACT

This paper is aimed at performing a group of experiments to evaluate the sensitivity to cumulus and microphysics schemes, as represented in numerical simulations of the Weather Research and Forecasting (WRF) model. The convective schemes of Kain-Fritsch (KF), Betts-Miller-Janjic (BMJ), Grell-Devenyi (GD), Grell-Freita (GF), Grell 3D (G3D), Tiedtke and New Tiedtke (NT) were tested in association with the microphysics schemes of Kessler, Purdue Lin, WSM3, WSM5, WSM6, ETA (Ferrier) and Goddard (totaling forty-nine experiments) in order to identify the combination which best represents the cumulative rainfall distribution in the Paraíba do Sul watershed. In order to evaluate the best performance experiments, they were submitted to statistical tests of bias (BIAS), root mean square error (RMSE), absolute mean error (MAE) and Coefficient of Determination (R2). Results show that combinations WSM5 and GD; Goddard and G3D; Perdue Lin and G3D; WSM5 and G3D form a group of four physical configurations statistically similar and able to predict well the mean rainfall in the Paraiba do Sul watershed. It was noticed also that the cumulus scheme has a greater weight than microphysics in rainfall simulations being GD3 the best performing.

Keywords: Atmospheric modeling system; Rainfall simulation; Convective Boundary Condition; Cloud microphysics

RESUMO

Este trabalho tem como objetivo realizar um conjunto de experimentos para avaliar a sensibilidade a esquemas cumulus e microfísicos, representados em simulações numéricas do modelo Weather Research and Forecasting (WRF). Os esquemas convectivos de Kain-Fritsch (KF), Betts-Miller-Janjic (BMJ), Grell-Devenyi (GD), Grell-Freita (GF), Grell 3D (G3D), Tiedtke e New Tiedtke (NT) foram testados em associação com os esquemas microfísicos de Kessler, Purdue Lin, WSM3, WSM5, WSM6, ETA (Ferrier) e Goddard (totalizando quarenta e nove experimentos) com a finalidade de identificar a combinação que melhor representa a distribuição acumulada de chuvas na bacia do Paraíba do Sul. Os esquemas de camada limite planetária, camada superficial, radiação de onda longa e radiação de onda curta foram definidos a partir de quatro experimentos configurados com parametrizações físicas já utilizadas na mesma região, e disponíveis na literatura. O modelo Global Forecast System (GFS) foi usado como dados de condição de contorno lateral para o procedimento de downscaling, e a resolução horizontal utilizada foi de 0,05° (~5,5km) na grade mais fina. Os experimentos foram realizados para o período de tempo entre 02 e 06 de janeiro de 2019, por ser o período de maior instabilidade média, registrado pelas 19 estações automáticas do Instituto Nacional de Meteorologia (INMET), distribuídas na bacia para o ano de 2018/ verão 2019. Para avaliar os experimentos de melhor desempenho, eles foram submetidos aos testes estatísticos de viés (BIAS), raiz quadrada do erro médio (RMSE), erro médio absoluto (MAE) e coeficiente de determinação (R2). Os resultados mostram que as combinações WSM5 e GD; Goddard e G3D; Perdue Lin e G3D; WSM5 e G3D formam um conjunto de quatro configurações físicas estatisticamente semelhantes e capazes de prever bem a precipitação média na bacia do Paraíba do Sul. Percebeu-se também que o esquema cumulus tem um peso maior que a microfísica nas simulações de chuva sendo GD3 o de melhor desempenho.

Palavras-chave: Modelagem atmosférica; Simulação de chuva; Condição de Contorno Convectiva; Microfísica de nuvens

1 INTRODUCTION

Currently atmospheric models are executed from a sophisticated set of physical parameterizations which considers atmospheric physics processes in an increasingly detailed way (LIU *et al*., 2018). Physical parametrization schemes are simplified formulations rather than complex theoretical models for solving the terms associated with turbulent momentum, heat and humidity flux. They are important components of numerical models, performing an important role in determining model behavior (GUNWANI; MOHAN, 2017).

Weather Research and Forecasting model (WRF) coupled schemes are: the microphysics, the longwave radiation, the shortwave radiation, cumulus, the

planetary boundary layer (PBL), the surface layer, and the surface model of the earth. Microphysics includes explicit processes of water vapor, cloud and precipitation. Radiation schemes deal with atmospheric heating due to the absorption, emission, and scattering phenomena and longwave and shortwave surface radiation for the calculation of ground temperature. The cumulus scheme is responsible for sub-grid effects, convection, and vertical distribution of moisture and heat. Surface layer schemes calculate friction velocities and exchange coefficients. Land surface schemes provide heat and moisture flows over land and sea-ice points. Planetary boundary layer schemes are responsible for turbulent mixing across the entire network column (SKAMAROCK *et al*., 2019).

Due to this large number of parameters to be inserted in the model, it is a recurring activity in the literature to resort to sensitivity tests in order to identify a set of schemes which efficiently respond to the meteorological and spatial variables for each case and region, being these tests empirically proposed, or even by trial and error (DI *et al*., 2015). The goal of this type of study is to use different combinations of parameters in order to understand how the variations in schemes associations affect the simulation of specific processes.

Mohan *et al*. (2018) used the WRF model to simulate a heavy rainfall event in southeast India and studied the sensitivity to microphysics parametrization, observing better results using the Thompson scheme. Avolio and Stefano (2018) simulated a heavy rainfall event in southern Italy using WRF and performed sensitivity tests with twelve different parametrizations and verified 156 rain gauges over the area of interest, finding that non-local Planetary Boundary Layer (PBL) scheme shows best performances.

Yang *et al*. (2019) performed a sensitivity analysis of raindrop size distribution parametrizations in WRF with three different microphysics parameterizations and obtained better accuracy using the Thompson aerosol-aware microphysics scheme comparing data for approximately 100 rainfall simulation events in Chilbolton, UK (United Kingdom).

Considering studies performed in Brazil, Comin *et al.* (2020) studied extreme rainfall events observed between May 20th and 30th 2017 in Brazil, on the east coast of NEB. It was investigated the results of 24 experiments with WRF different PBL implementations comparing them against weather station data and precipitation estimates by the Tropical Rainfall Measurement Mission (TRMM, Simpson *et al.* 1996). It was found that the Morrison scheme performed better compared to the other schemes.

The combination of all schemes inserted in WRF generate, many number of different parametrization possibilities, which highlighting the obstacle associated with the task of defining a parameterization that represents a precisely local atmospheric phenomenon (SALES *et at,*. 2021). Each new version of model relies on the implementation of new schemes, which increases the number of combinations in relation to the previous version.

The present study was carried out in the Paraíba do Sul River watershed in Brazil, which has an area of approximately 62,074 km² extending over the states of São Paulo (14,510 km²), Rio de Janeiro (26,851 km²) and Minas Gerais (20,713 km²). This watershed encompasses 184 municipalities, of which 88 in Minas Gerais, 57 in the state of Rio de Janeiro and 39 in the state of São Paulo (CEIVAP, 2019). Since rainfall is mostly recorded from stations located in the urban areas of major population agglomerations, it is justified to create computational models for precipitation effects evaluation along the watershed.

For the microphysics and convection schemes, in this paper 49 numeric experiments are performed combining the Kesseler, Purdue Lin, WSM3, WSM5, WSM6, Eta (Ferrrier) and Goddard microphysics schemes, together with Kain-Fritsch (KF), Betts-Miller-Janjic (BMJ), Grell-Devenyi (GD), Grell-Freitas (GF), Grell3D (G3D), Tiedtke and New Tiedtke (NT) convective schemes. The objective was to evaluate the performance of each experiment and determining the best mean performance combination across the watershed. The methodology was to calculate the statistical measures of bias, the mean absolute error, the root mean squared error and the

coefficient of determination against measurements available from 19 Meteorological Automatic Stations. Then, finally the results were analyzed pointing out a small group of microphysics and convective schemes combinations (WSM5 and GD; Goddard and G3D; Perdue Lin and G3D; WSM5 and G3D) to be used in the WRF setup with closer results to measurements. It was also possible to notice that the cumulus scheme has a greater weight than microphysics in rainfall simulations being GD3 the best performing.

2 MATERIAL AND METHODS

2.1 WRF model description

The WRF is a flexible public domain model that can be used with spatial resolutions from tens of meters to thousands of kilometers, composed of two dynamic solvers the NMM (Nonhydrostatic Mesoscale Model) and ARW (Advanced Research WRF). The WRF-ARW version 4, available from the WRF website was used in the present study (WRF, 2019).

This model supports the initial and lateral boundary conditions that are obtained in GRIB format from various global models, such as: ERA-Interim reanalysis data, North American Model (NAM), Rapid Update Cycle (RUC), Agricultural Meteorology (AGRMET) from the Air Force Weather Agency - AFWA), Global Forecast System (GFS) analysis products, and others, as described by Wang *et al*. (2019).

Static geographical data are required for model grids, such as soil layers, land use category, terrain altitude, average annual soil temperature, monthly vegetation fraction, and monthly albedo. The global data sets for each of these fields are provided through the WRF download page at http://www2.mmm.ucar.edu/wrf/users/download/get_sources_wps_geog.html. Many of the datasets are available in one resolution only, but others are available to be downloaded either with high or low resolutions. A higher data resolution implies in higher computational costs, though the computational cost will in fact be defined by the grid resolution used by modeler.

For the representation of the surface model, the user can choose one from a set of three cartographic projections that seeks to offer the best possible description of the surface for each latitude range, where the Polar Projection is indicated for high latitude domains, Lambert's Conformal Projection for domains of medium latitude and Mercator Projection is suitable for low latitude domains. The Cylindrical Conformal is an alternative projection suitable to be used for global simulations, although it can also be used for regional domains anywhere on the planet. It is important to point out that although the WRF model is designed for regional analysis, it has the flexibility to be used also for local studies. To do so, it allows multiple domains (nesting) which are used for the downscaling process, and therefore minimizing errors (WARNER, 2010).

For vertical coordinates the model uses a hybrid sigma pressure vertical coordinate system, defined in relation to the top pressure of the atmosphere (upper boundary), and it considers variations in topography, that promote variations in hydrostatic pressure along the column. In the version 4 of the WRF model, the vertical coordinate has been generalized to allow the influence of the terrain on the coordinate surfaces which are quickly removed with increasing height above the surface, so that the higher layers receive less influence from the topography (SKAMAROCK *et al*., 2019).

The WRF-ARW supports an Arakawa-C grid format, where the time integration is performed with 2nd and 3rd order Runge-Kutta schemes and has a high order advection scheme (SKAMAROCK *et al*., 2019). The interactions between the atmosphere and surface are described from the governing dynamic equations solved by the solvers.

The WRF Pre-Processing System (WPS) module is intended to prepare the input for the real processing program, and it is composed of three applications which are set up in the "namelist.wps" file: (a) geogrid: defines the domains and interpolates static geographic data, available in WPS binary format, for the grids; (b) unbrib: extracts weather data for initial and lateral boundary conditions, distributed in GRIB format and is provided for any global model; (c) metgrid: horizontally interpolates the weather data extracted by ungrib to the grid defined by the "geogrid".

The WRF module is divided split in two submodules. The first is the "real", which performs a vertical interpolation of atmospheric data previously interpolated horizontally by the "metgrid", thus completing the preprocessing step. The last application to be run is the "wrf" which is responsible for using all the data prepared in the previous steps, performing the simulation from the definition of the physical parameters already set up in the "namelist.input" file (WANG *et al*., 2019).

Post-processing can be performed in several programming languages being the most common NCL, WRF-Python and R language. In this study post-processing was performed in R v.3.6.0 (R-PROJECT, 2019), for extraction and manipulation of data generated by the model, as well as mathematical and statistical operations for time series analysis. To produce the maps and to represent geoscientific information, the software QGIS v.3.8.0 was used (QGIS, 2019).

2.2 WRF experiment design and data

The model was set up with two nested domains where the external domain (D1) is composed of a 67 x 54 grid with spatial resolution of $\Delta x = \Delta y = 0.15°$ (~ 16.5 km), while the internal domain (D2) is composed of a grid of 120 x 81 cells with spatial resolution of $\Delta x = \Delta y = 0.05°$ (~ 5.5 km). The coordinates of the central point of the domains are 43.550° W / 22.077° S, with the nesting arrangement being constructed so that the finer grid covers the entire area of the Paraíba do Sul River watershed. The coordinate system used was geographic and the projection was the Cylindrical Conformal. In Figure 1 it is shown the nesting of the domains D1 and D2.

The vertical profile of the model was configured for 35 "sigma" layers at 5000 Pa to the top of the atmosphere, thus setting the vertical boundary condition for model integration. The integration time interval was 90 s and the model output setup defined to save data at every hour. Static data was defined from the standard "high resolution" option provided by the model.

The initial and lateral boundary conditions for the experiments were obtained from the numerical GFS analysis data provided by the National Centers for Environmental Prediction (NCEP), which holds the atmospheric information with a 6h temporal resolution and a 0.25° spatial resolution.

Figure 1 – Location of Paraíba do Sul River watershed and computational domain representation
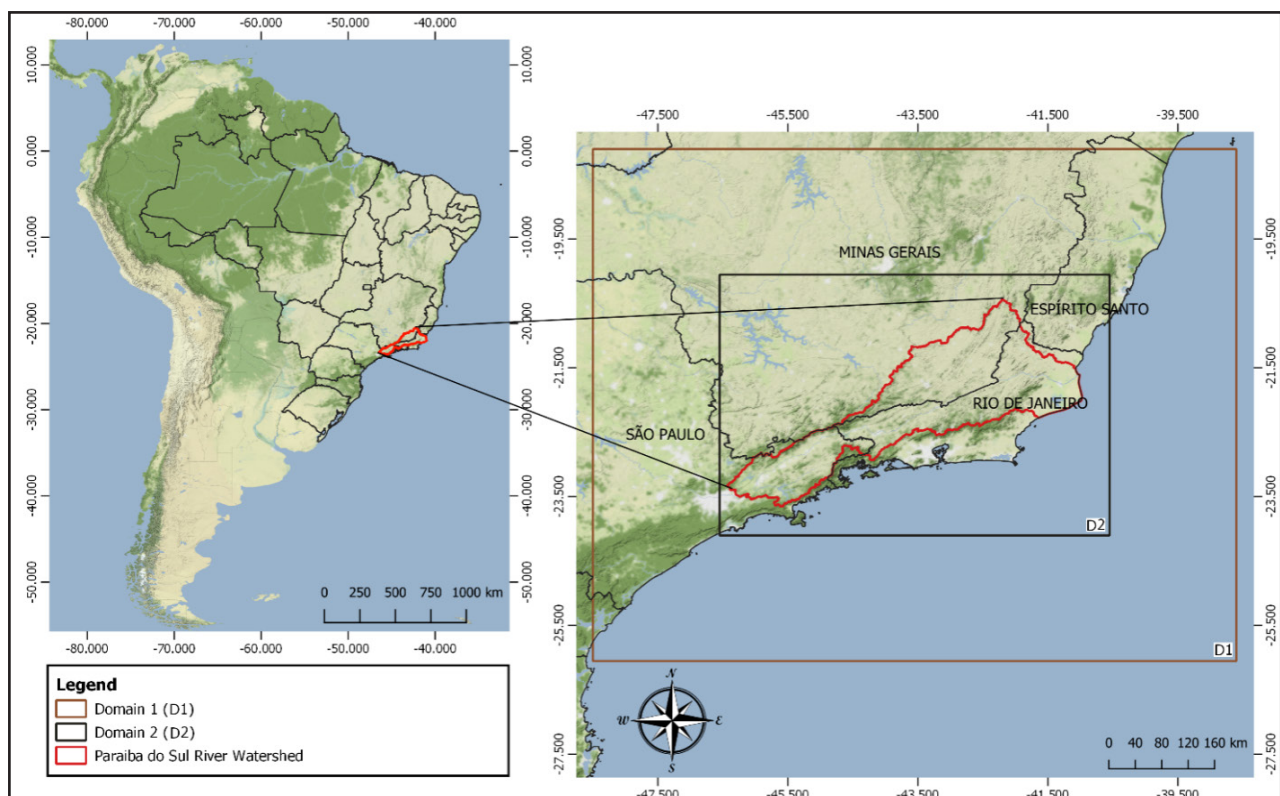
Source: Author's (2022)

To determine the period of simulation, it was used a methodology like the study of Di *et al*. (2015), who sought into the Chinese summer period, the most unstable days, to perform their experiments. Thus, it was chosen to be simulated the Brazilian summer period between December 21th, 2018 and March 20th, 2019, since this period is characteristic for receiving the highest amount of rainfall in the tropical regime.

Figure 2 – Distribution of INMET's meteorological automatic stations within the Paraíba do Sul watershed

| ID	INMET Automatic Station	State	Latitude	Longitude
1	Campos - São Tomé	Rio de Janeiro	-22.041647	-41.051871
2	Campos dos Goytacazes	Rio de Janeiro	-21.714767	-41.344017
3	Cambuci	Rio de Janeiro	-21.587729	-41.958327
4	Muriaé	Minas Gerais	-21.104867	-42.375904
5	Santa Maria Madalena	Rio de Janeiro	-21.950592	-42.010489
6	Carmo	Rio de Janeiro	-21.938744	-42.600936
7	Teresópolis - Parque Nacional	Rio de Janeiro	-22.448922	-42.987146
8	Três Rios	Rio de Janeiro	-22.098391	-43.208574
9	Juiz de Fora	Rio de Janeiro	-21.769965	-43.364329
10	Petrópolis	Rio de Janeiro	-22.464889	-43.291505
11	Valença	Rio de Janeiro	-22.358094	-43.695656
12	Rio Claro (Passa Três)	Rio de Janeiro	-22.653579	-44.040916
13	Resende	Rio de Janeiro	-22.450924	-44.444786
14	Itatiaia - Parque Nacional	Rio de Janeiro	-22.373944	-44.703111
15	Cachoeira Paulista	São Paulo	-22.689001	-45.005444
16	Taubaté	São Paulo	-23.041668	-45.520841
17	Coronel Pacheco	Minas Gerais	-21.546728	-43.261029
18	Nova Friburgo	Rio de Janeiro	-22.334839	-42.676932
19	São Luis do Paraitinga	São Paulo	-23.228362	-45.417055

Source: Author's (2022)

For the identification of the date of greatest instability, it was observed the day with the highest intensity of mean rainfall, recorded by 19 automatic stations from the Brazilian National Institute of Meteorology (INMET), randomly distributed within the Paraíba do Sul River watershed as shown in Figure 2. Data recorded by these stations are of public domain and are available at website http://www.inmet.gov.br/portal/. Such sets of data were subsequently used for model evaluation.

In order to determine the average rainfall into the watershed it was performed the arithmetic sum of the cumulative rainfall at all automatic stations installed, divided by the number of stations observed. It is possible to observe that the date with the highest rainfall was January 4th, 2019, with an average daily rainfall of 28.6 mm, as shown in Figure 3. Two days before and after January 4th, 2019, were considered in the simulation, in order to ensure that the model observes the entire period of

instability. The simulations started at 0000 UTC, January 2nd, 2019 and ended at 0000 UTC, January 6th, 2019, being excluded from the analysis the spin-up of the first 24h of simulation corresponding to January 2nd, 2019, in order to eliminate the instabilities related to the beginning of the simulation.

Figure 3 – Mean rainfall from 19 INMET automatic stations into the Paraíba do Sul watershed for 2018/2019 summer
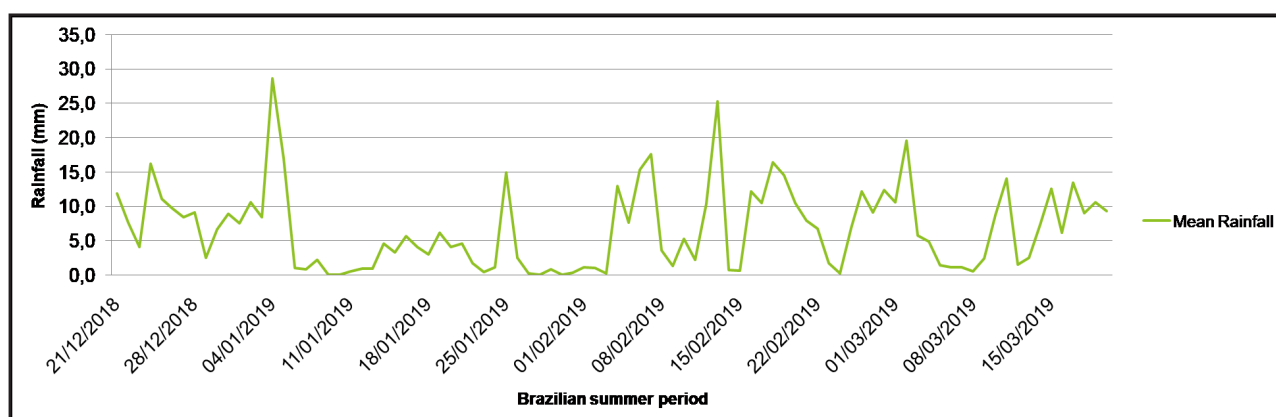
Source: Author's (2022)

2.3 WRF Physical Parameterizations sets

Even though the precipitation is originated from the interaction of all the schemes that composes the physical parameterization, Liu *et al*. (2018) consider the convection and microphysical parameterization schemes the two most important components related to precipitation and cloud simulations in atmospheric models. The total precipitation is a sum of convective (cumulus) and non-convective (microphysical) rainfall (WANG *et al*., 2019).

Using this concept, in this study with focus on the Paraiba do Sul watershed region are considered planetary boundary layer (PBL), surface layer, land surface, longwave radiation and shortwave radiation schemes, which have been defined based on tests performed with the parameters described in the studies of Bender

(2012), Silva *et al*. (2016), Silva *et al*. (2017) and Souza *et al*. (2017), in which was used the (WRF-ARW).

Silva *et al*. (2017) examined the characterization of atmospheric thermodynamic conditions and investigated the triggering dynamics of rain events on two specific days, November 29th and December 12th, 2016, in which heavy rainfall forecasts were registered for the Rio de Janeiro Metropolitan Region. Bender (2012) assessed the ability of the WRF-ARW model to effectively perform weather forecasting in São Paulo by evaluating temperature and precipitation parameters from April 2010 to March 2011. Silva *et al*. (2016) sought to evaluate the performance of atmospheric indicators in rainfall events that occurred in the city of Rio de Janeiro, in the period 1997-2012, with the objective of identifying which of them presented greater reliability in identifying favorable atmospheric conditions, as well as the occurrence of severe rainfall. The study of Souza *et al*. (2017) seeks to associate the influence of urban heat islands in the convective processes of rain formation, able to modify the rainfall regime of the metropolitan region of São Paulo on January 24th, 2014, November 26th, 2014 and December 22th, 2014.

Once identified the most representative simulation among the experiments already performed in the watershed, this study intends to make combinations of microphysical and convective schemes to identify the best representation of the precipitation. All possible combinations were performed between the microphysics schemes described in Table 1 associated with cumulus schemes described in Table 2, totaling 49 experiments, in order to determine the best performance combination.

Table 1 – Microphysics parameterization options tested Wang *et al.* (2019) and Skamarock *et al.* (2019). The variables represented by each microphysical parameterization scheme are: mixing ratio for water vapor (Qv), mixing ratios for rain water (Qr), mixing ratios for cloud water (Qc), mixing ratios for snow (Qs), mixing ratios for ice (Qi) and mixing ratios for graupel (Qg)

Scheme	Mass Variables	Characteristics	Reference
Kessler	Qv Qc Qr	Commonly used in idealized cloud modeling studies; Process of production, fall, and evaporation of rain; Accretion and auto-conversion of cloud water; Production of cloud water from condensation.	Kessler (1969)
Purdue Lin	Qv Qc Qr Qi Qs Qg	Six classes of moisture variables are included: water vapor, cloud water, rain, cloud ice, snow and graupel; Suitable for real-data high-resolution simulations.	Chen and Sun (2002)
WSM3	Qv Qc Qr	Three categories of moist variables: water vapor, cloud water/ice, and rain/snow; Suitable for mesoscale grid sizes.	Hong; Dudhia; Chen (2004)
WSM5	Que Qc Qr Qi Qs	Efficient in intermediate grids between the mesoscale and cloud-resolving grids; Allows for mixed-phase processes and super-cooled water.	Hong; Dudhia; Chen (2004)
Eta (Ferrier)	Qv Qc Qr Qs (Qt)	The operational microphysics in NCEP models; Scheme with diagnostic mixed-phase processes.	Rogers; Black; Ferrier; Lin; Parrish; Di Mego (2001)
WSM6	Qv Qc Qr Qi Qs Qg	Including graupel processes; Suitable for high-resolution simulations.	Hong and Lim (2006)
Goddard	Qv Qc Qr Qi Qs Qg	Scheme with ice, snow and graupel processes; Suitable for high-resolution simulations.	Tao; Simpson; McCumber (1989)

Source: Author's (2022)

Table 2 – Cumulus parameterization options tested Wang *et al*. (2019) and Skamarock *et al*. (2019). The variables represented by each microphysical parameterization scheme are: mixing ratios for rain water (Qr), mixing ratios for cloud water (Qc), mixing ratios for snow (Qs) and mixing ratios for ice (Qi)

Scheme	Moisture Tendencies	Momentum Tendencies	Shallow Convection	Characteristics	Reference
Kain-Fritsch (KF)	Qc Qr Qi Qs	No	Yes	Deep and shallow convection sub-grid scheme using a mass flux approach with downdrafts and CAPE removal time scale.	Kain (2004)
Betts-Miller-Janjic (BMJ)	-	No	Yes	Operational Eta scheme; Column moist adjustment scheme relaxing towards a well-mixed profile.	Janjic (1994)
Grell-Devenyi (GD)	Qc Qi	No	Yes	Multi-closure, multi-parameter, ensemble method.	Grell and Devenyi (2002)
Grell-Freitas (GF)	Qc Qi	No	Yes	An improved GD scheme that tries to smooth the transition to cloud-resolving scales.	Grell and Freitas (2014)
Grell 3D (G3D)	Qc Qi	No	Yes	Improved version of the GD scheme that may also be used on high resolution.	Grell (1993) Grell and Devenyi (2002)
Tiedtke	Qc Qi	Yes	Yes	Mass-flux type scheme with CAPE removal time scale, shallow component and momentum transport.	Tiedtke (1989), Zhang *et al*. (2011)
New Tiedtke (TD)	Qc Qi	Yes	Yes	Entrainment and detrainment rates for all types of convection, conversion from cloud water/ice to rain/ snow and options for momentum transport	Zhang and Wang (2016)

Source: Author's (2022)

2.4 Verification methods

There are several points to be considered in the validation of a model and the methodology imposed. Besides, the metrics may change according to the application of interest. Ferreira *et al*. (2008) describe Five different ways to validate a model: (a) comparison with the results of an equivalent model; (b) verification of balances expressing the conservation of mass and energy; (c) comparison with results of different numerical models in the design; (d) comparison between results of alternative formulations of the same model; and (e) comparison of model predictions with observations generated from physical stations. In the present paper it is used an association of items (d) and (e), as it proposes to test several parameterizations imposed on the same model, in relation to the data observed by the INMET physical stations, as well as to establish a comparison between simulations.

Data from the INMET automatic stations were used, corresponding to an hourly observed time series. In order to obtain predict time series (model results), the coordinates of the INMET automatic stations were used in the computation of the precipitation pixel value at every hour.

Three error metrics were used to represent the deviations between the predict (simulated) and the observed values (INMET station) and additionally it was used the coefficient of determination to check the model performance. Equations are presented as following:

$$Bias = \frac{1}{N}\sum_{i=1}^{N}\Phi_i' \tag{1}$$

$$RMSE = \left[\frac{1}{N}\sum_{i=1}^{N}(\Phi_i')^2\right]^{1/2} \tag{2}$$

$$MAE = \frac{1}{N}\sum_{i=1}^{N}|\Phi_i'| \tag{3}$$

$$R^2 = \left(\frac{\sum_{i=1}^{N}(\Phi_{i,p}-\overline{\Phi}_{i,p})\cdot(\Phi_{i,obs}-\overline{\Phi}_{i,obs})}{\sqrt{\sum_{i=1}^{N}(\Phi_{i,p}-\overline{\Phi}_{i,p})^2}\cdot\sqrt{\sum_{i=1}^{N}(\Phi_{i,obs}-\overline{\Phi}_{i,obs})^2}}\right)^2 \tag{4}$$

Where represents the difference between the mean predicted values (from the model) and the mean observed values (from the INMET stations), with = 1,2,..., *N*, where N represents the number of observations. In the case of the present study, N=73, referring to the 72 hours of simulation added the initial condition.

The BIAS represents the distance between simulated precipitation and observations, where positive values indicate that the model tends to overestimate the observed values, while negative values imply that model tends to underestimate them. The root mean square error (RMSE) is a measure of the magnitude of the mean error between simulated and observed values, representing the standard deviation of differences. The mean absolute error (MAE) represents the absolute mean deviation of simulated precipitation from observations. For all error measures the best values are represented by their proximity to zero, that indicates a smaller distance between simulated and observed values, which implies a better fit.

Additionally, it was calculated the coefficient of determination (R^2) that gives the degree of linearity between simulated precipitation and the observations. It ranges from 0 to 1 being expressed in percentage terms, where 1 represents a perfect adjust.

3 RESULTS AND DISCUSSION

3.1 Sensitivity analysis assessment of physical parameterization using previous studies in the region

The physical parameters tested were chosen from studies available in the literature for the region of interest, the Paraíba do Sul River Watershed. This initiative has a double goal, the first one is to provide a comparison with the experiments already carried out, and the second one is to promote a critical reflection, as well as an update on the previously proposed parametrizations.

Four studies were found, which are described in section 2.3, and describe all seven schemes that make up the physical parameters: microphysics, cumulus (or convective),

planetary boundary layer (PBL), surface layer, land surface, longwave and shortwave radiation. The summary of physical parameterization used is shown in Table 3.

The four physical parameterizations found (Table 3) were tested according to the model designed (section 2.2) and analyzed using to the statistical criteria described in the methodology i.e. the error metrics previously described (section 2.4).

Table 3 – Physical parameterizations found in the literature for studies conducted with WRF-ARW, in the States of Rio de Janeiro and São Paulo, Brazil, between 2012 and 2017

Experiment	Study	Microphysics	Cumulus	PBL	Surface Layer	Land Surface	Long wave	Short wave
1	SILVA *et al*. (2017)	WSM3	KF	YSU	MM5 Monin–Obuckov	Noah land surface model	RRTM	Dudhia
2	BENDER (2012)	WSM3	GD	YSU	MM5 Similarity Scheme	Noah land surface model	RRTM	Dudhia
3	SILVA *et al*. (2016)	WSM3	GD	MYJ	ETA - Similarity Scheme	Noah land surface model	RRTM	Dudhia
4	SOUZA; RANGEL; CATALDI (2017)	WSM3	KF	YSU	MM5 Similarity Scheme	Noah land surface model	RRTM	Dudhia

Source: Author's (2022)

Statistical tests were performed from the hourly average of all stations and all experiments. The analyzes were based on accumulated time series, and the objective was to verify the behavior of total rainfall in the watershed. The summary of the results found are shown in Table 4. The best values obtained are shown in boldface.

Table 4 – Result of experiments performed with the physical parameterizations previously used in the region of interest, Paraíba do Sul River Watershed

Experiment	BIAS (mm)	RMSE (mm)	MAE (mm)
1	8.99	11.00	9.04
2	5.96	8.57	6.12
3	4.05*	6.82*	4.47*
4	8.25	10.19	8.32

Source: Author's (2022)

*Best results

From the imposed methodology, experiment number 3 was the best result for all the tests performed, being the one that best represented the precipitation for the proposed period and model design. Positive values for the BIAS in all experiments demonstrate the tendency of the model to overestimate precipitation. MAE result associated with RMSE indicates that experiment number 3 corresponds to the most adjusted model. It is important to highlight that since it is a cumulative analysis, the deviations are added over time, tending to be larger in the final periods.

3.2 Sensitivity Analysis Assessment of Cumulus and Microphysics parameterization

Once determined that experiment 3 had the best performance, 49 experiments were proposed in order to consider all possible associations between the seven microphysics schemes and the seven convective schemes, previously described in section 2.3. It was used the PBL (Planetary Boundary Layer), surface layer, land surface, shortwave radiation, and longwave radiation schemes of experiment 3, as described in Table 3.

The configurations of each convective and microphysical scheme association are identified in Table 5. Since experiment 3 already represents an association between convective and microphysical schemes, 48 possible associations are presented in the Table. The experiments were identified from experiment number 5 on since the first

four experiments have already been described in the Tables 3 and 5. The corresponding statistical comparison results are shown in Table 4.

The joint analysis of Tables 5 and 6 shows a group of 4 best performing combinations, with numerically similar results (the analysis was based on cumulative time series). Thus experiments 24, 41, 43 and 45 stand out from the rest, and form the group of the smaller deviations.

Table 5 A – Experiments set up combining seven microphysical schemes and seven cumulus schemes

Experiment	Microphysics	Cumulus
5	WSM6	GD
6	Eta (Ferrier)	GD
7	Goddard	GD
8	Kessler	GD
9	Purdue Lin	GD
10	WSM6	KF
11	Eta (Ferrier)	KF
12	Goddard	KF
13	Kessler	KF
14	Purdue Lin	KF
15	WSM3	KF
16	WSM6	GF
17	Eta (Ferrier)	GF
18	Goddard	GF
19	Kessler	GF
20	Purdue Lin	GF

Source: Author's (2022)

Table 5 B – Experiments set up combining seven microphysical schemes and seven cumulus schemes

Experiment	Microphysics	Cumulus
21	WSM3	GF
22	WSM5	GD
23	WSM5	KF
24	WSM5	GF
25	Eta (Ferrier)	NT
26	Eta (Ferrier)	BMJ
27	Eta (Ferrier)	G3D
28	Eta (Ferrier)	Tiedtke
29	Goddard	BMJ
30	Kessler	BMJ
31	Purdue Lin	BMJ
32	WSM3	BMJ
33	WSM5	BMJ
34	WSM6	BMJ
35	Goddard	NT
36	Kessler	NT

Source: Author's (2022)

Table 5 C – Experiments set up combining seven microphysical schemes and seven cumulus schemes

Experiment	Microphysics	Cumulus
37	Purdue Lin	NT
38	WSM3	NT
39	WSM5	NT
40	WSM6	NT
41	Goddard	G3D
42	Kessler	G3D

Table 5 C – Experiments set up combining seven microphysical schemes and seven cumulus schemes

(Conclusion)

Experiment	Microphysics	Cumulus
43	Purdue Lin	G3D
44	WSM3	G3D
45	WSM5	G3D
46	WSM6	G3D
47	Goddard	Tiedtke
48	Kessler	Tiedtke
49	Purdue Lin	Tiedtke
50	WSM3	Tiedtke
51	WSM5	Tiedtke
52	WSM6	Tiedtke

Source: Author's (2022)

Table 6 – Results comparison for the experiments performed with the combination of seven microphysical schemes and seven cumulus schemes (cumulative mean rainfall analysis)

(Continue)

Experiment	BIAS (mm)	RMSE (mm)	MAE (mm)	Experiment	BIAS (mm)	RMSE (mm)	MAE (mm)	Experiment	BIAS (mm)	RMSE (mm)	MAE (mm)
5	5.72	8.33	5.85	21	-3.89	6.19	4.37	37	-9.27	12.01	9.27
6	4.58	6.87	4.87	22	4.26	6.83	4.64	38	-4.71	6.79	4.86
7	3.40	6.48	4.79	23	13.20	16.31	13.35	39	-4.83	6.84	4.92
8	3.74	6.47	4.49	24	-1.72*	2.84*	2.18*	40	-6.48	9.52	6.59
9	5.11	8.00	5.30	25	-8.31	10.74	8.31	41	-0.86*	3.32*	2.43*
10	13.72	16.86	13.85	26	-16.26	21.48	16.26	42	-1.72	4.10	2.86
11	11.55	13.88	11.68	27	-3.46	5.53	3.78	43	-0.72*	3.36*	2.44*
12	8.30	10.34	8.40	28	-11.49	14.42	11.49	44	1.32	4.34	2.87
13	14.91	18.03	15.07	29	-14.47	18.70	14.47	45	0.28*	3.33*	2.45*
14	18.74	22.97	18.89	30	-15.44	19.82	15.44	46	-1.00	3.58	2.74

Table 6 – Results comparison for the experiments performed with the combination of seven microphysical schemes and seven cumulus schemes (cumulative mean rainfall analysis)

(Conclusion)

Experiment	BIAS (mm)	RMSE (mm)	MAE (mm)	Experiment	BIAS (mm)	RMSE (mm)	MAE (mm)	Experiment	BIAS (mm)	RMSE (mm)	MAE (mm)
15	10.02	12.50	10.21	31	-16.94	22.18	16.94	47	-13.48	17.48	13.48
16	-4.44	7.35	5.09	32	-17.87	23.33	17.87	48	-10.05	12.32	10.05
17	-8.05	10.12	8.05	33	-17.20	22.52	17.20	49	-10.71	13.03	10.71
18	-7.42	9.79	7.42	34	-17.19	22.47	17.19	50	-11.89	14.51	11.89
19	8.81	10.95	9.00	35	-9.85	13.06	9.85	51	-10.91	13.39	10.91
20	1.35	3.75	3.20	36	-9.05	11.88	9.05	52	-11.88	14.78	11.88

Source: Author's (2022)

*Set of smaller deviations

Experiments 24, 41 and 43 presented negative BIAS which means that the model underestimated the result in relation to the observations data. Experiment 45 was the only one that had a positive result value, so it overestimated the observed data. Regarding the MAE metric, all four best-performing experiments had a mean deviation of 2.5 mm and regarding RMSE the magnitude of error was lower at 3.5 mm for all best-performing experiments. Thus, all tests observe a very significant adjustment of the model to this group. It is important to note that, for all the error metrics mentioned, only the deviation from the average time is considered, not necessarily implying the deviation achieved in the last simulation hour (after the 72 hours of simulation).

In order to observe the total precipitation behavior into the watershed along the simulation period, it was plotted the mean curves for the four best performing experiments and the cumulative mean curve observed at the INMET automatic stations, as shown in Figure 4. When analyzing the curves, it is possible to observe that they follow the same behavior, and consistently represent the cumulative precipitation into the watershed. Therefore, it is possible to observe that, from this analysis no major differences among best performing experiments.

It is important to observe that negative values of BIAS mentioned in Table 4,

mean that the predicted curve was kept under the curve with observed data, although after the 72 hours (final accumulated precipitation value) the value presented for all experiments are greater than observed values. In the other words the BIAS represents the mean behavior of the curve and not the total cumulative rainfall.

Figure 4 – 72 hours of cumulative mean curves of the 4 best simulations and average observed data (January 3rd-6th, 2019)
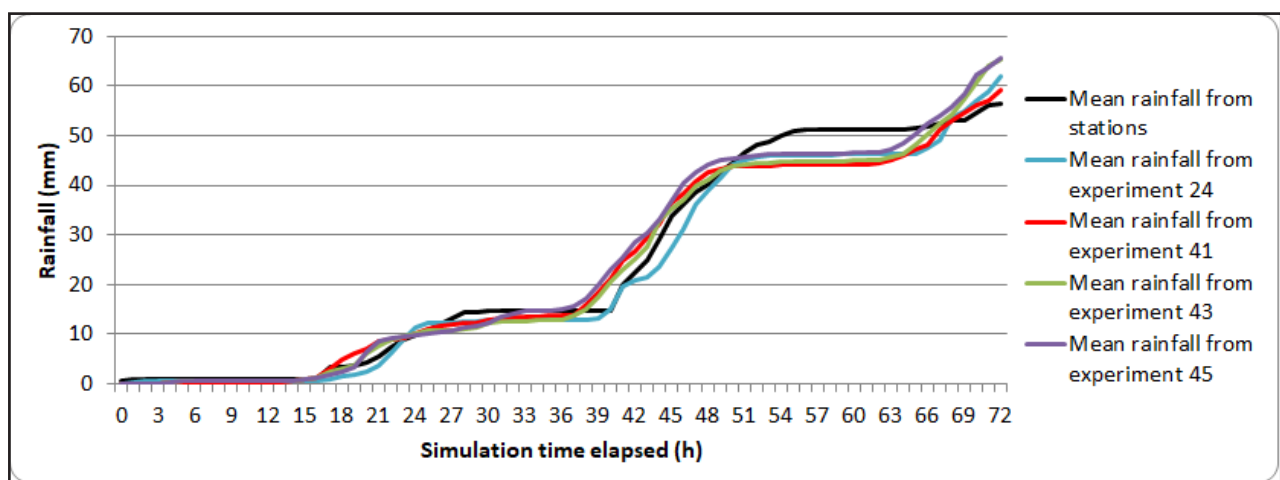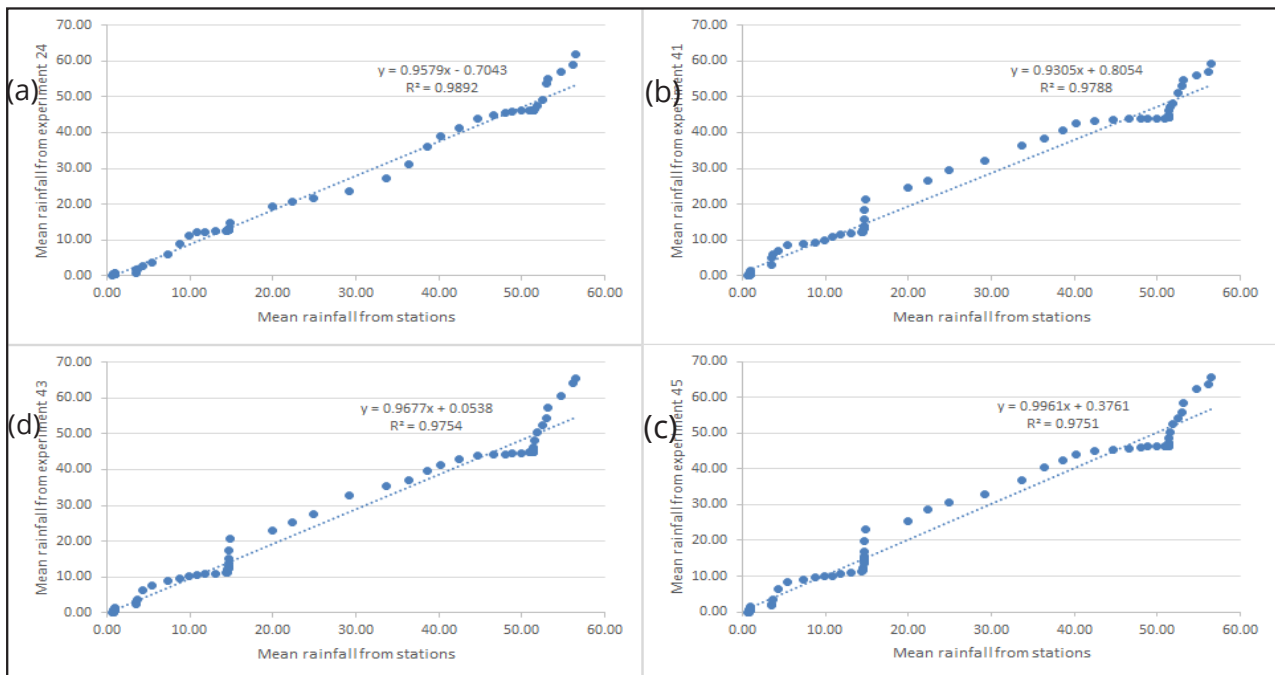

Source: Author's (2022)

The analysis of the linear correlation of the cumulative curves confirms the similar behavior of the curves visualized in Figure 4. The results of the linear correlation models present experiment 24 as the best fit of the curve, followed by experiments 41, 43 and 45, as can be seen in Figure 5. In all experiments, an R^2 above 0.97 was found, which means that the model explains the phenomenon in more than 97% of cases and resulting in a very significant adjustment. Therefore, analyzing only the coefficient of determination, no significant differences were observed between the four experiments mentioned, confirming the homogeneity of the group.

The group with the four best experiments can be classified according to the RMSE in association with coefficient of determination. In the other words, considering the magnitude of the error (smaller deviation) and the curve behavior. From this point of view the experiments could be classified in this order: 24, 41, 45 and 43 (from the best to worst),

even though the numerical difference is not really significant.

Since no significant difference was observed in the error metrics (mean deviation) and the coefficient of determination of the cumulative curves, the simulation that presents the total precipitation closest to the value measured at the stations, can be adopted as a better performing experiment (see hour 72 in Figure 4). The total accumulated precipitation in the simulation period for experiments 24, 41, 43 and 45 was 61.89, 59.22, 65.43 and 65.58, respectively and the accumulated precipitation observed in INMET stations was 56.42. So, experiment 41 can be adopted as the best performance, presenting a 5% deviation from the mean accumulated precipitation measured at stations.

Figure 5 - Dispersion plot of the best performing simulations (accumulated rainfall analyses)

Source: Author's (2022)

(a) Linear correlation between mean rainfall from INMET stations and mean rainfall from experiment 24.
(b) Linear correlation between mean rainfall from INMET stations and mean rainfall from experiment 41.
(c) Linear correlation between mean rainfall from INMET stations and mean rainfall from experiment 43.
(d) Linear correlation between mean rainfall from INMET stations and mean rainfall from experiment 45.

Although it is not the focus of this work, hourly analysis was conducted only from

the group with the best performance to evaluate them. Thus, using the hourly analysis of the precipitation behavior, as shown in Figure 6, it was possible to observe that the period of greatest instability occurred in the interval between the 40th and 57th hour of simulation, followed by a period of no rain until the 64th hour of simulation, and finally for a period of low average rainfall in the watershed of approximately 1.5 mm at the 70th hour. All experiments followed the observed curve (black line - mean rainfall from stations), including the period of greatest instability.

The error measures related to the hourly data were calculated where it was possible to observe that all experiments tended to overestimate the observed data (positive BIAS), with all experiments presenting MAE below 1 mm, as well as, RMSE close to 1 mm, the which represents a really low average hourly. Experiment 41 again stands out as the one with the best performance, presenting an RMSE value of 0.95 mm. The results of the error metrics can be seen in Table 7.

Table 7 – Results comparison for the best performing experiments (hourly mean rainfall analysis)

| Experiment	BIAS (mm)	MAE (mm)	RMSE (mm)
24	0.07	0.57	0.99
41	0.04*	0.63*	0.95*
43	0.12	0.72	1.04
45	0.13	0.78	1.10

Source: Author's (2022)

*Best results

So, within the above, the Goddard microphysics combination associated with the Grell 3D convective scheme (experiment 41) can be considered the one that best represented the average rainfall of the watershed, although the difference was not significant. Corroborating this result, Padilha (2011) observed in her study that the Goddard microphysics scheme was also the one that best represented rainfall when analyzing localized events of instabilities in the city of Rio de Janeiro. But, the authors in that study

tested only microphysics schemes.

Considering individually, the convective (or cumulus) results confirms the studies of Patel *et al.* (2019) and Mayor and Mesquita (2015), who using a grid spacing like the one proposed in this paper identified the cumulus scheme as a factor of greatest influence on precipitation simulation. The study of Rodriguéz *et al.* (2016), proposes variations only in the cumulus parameterization for rainfall forecast in the southern region of Brazil, recognizing this as the most relevant for this type of study. This information becomes relevant because establishes experimentally the importance of using and adjusting this scheme for the grid configured in this study (~5.5 km), and the region under analysis. About convective schemes, Skamarock *et al.* (2019) states that these are not used for grids of less than 4 km, since precipitation is solved only by microphysics, whereas for grids larger than 10 km this should be used. According to the author, the interval between 5 and 10 km (such as in this paper) is not mandatory and depends of application.

Figure 6 – 72 hours of hourly mean curves of the four best simulations and mean observed data (January 3rd-6th, 2019)
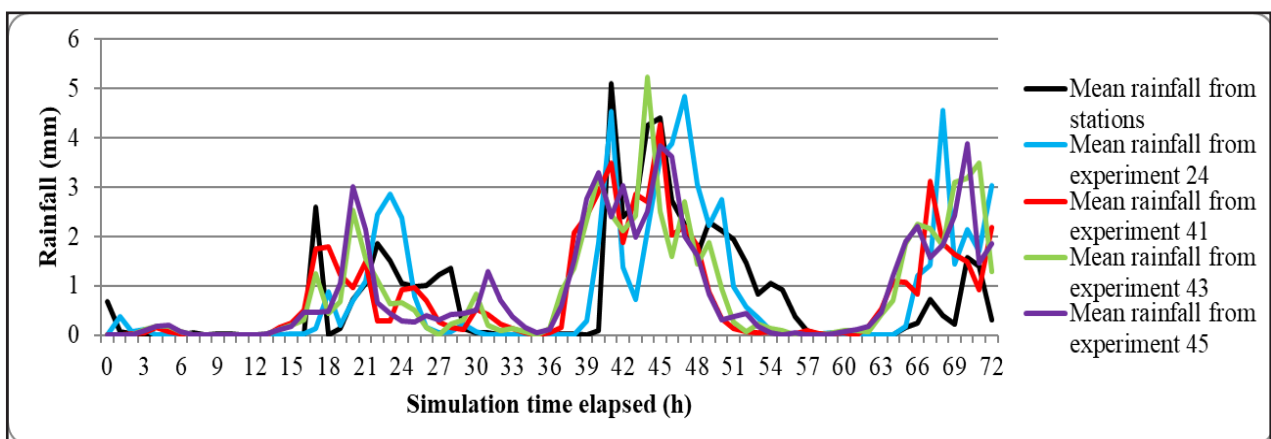
Source: Author's (2022)

The results showed that the Grell 3D convective scheme produced the smallest deviation for the region in all microphysical combinations, in contrast to the Betts-Miller-Janjic, Kain–Fritsch and Tiedtke schemes, in this order, which yielded the largest

deviations. The study of Calado *et al*. (2018) for the same watershed concluded that the Betts-Miller-Janjic and Kain-Fritsch schemes performed better, however, the mentioned study did not consider all the convective schemes tested in the present study and did not use the WRF model.

Regarding the microphysical schemes, it was observed that these did not produce large deviations when analyzed separately. Analyzing the experiments in which the seven microphysics schemes are associated with the best performing convective scheme (Grell 3D), it was observed that the largest deviation was found for the Eta (Ferrier) microphysics, as opposed to the work of Calado *et al*. (2018) that led to the best result for the region using this scheme.

The number of Meteorological Stations over the Paraíba do Sul river watershed is very small and the spatial interpolation of measured values are not able to represent very well the phenomena. But, for the sake of knowledge and since there is no better solution, it will be used comparing visually the graphs with interpolated measurement and simulated values. In order to analyze the spatialization of the accumulated period precipitation (total cumulative precipitation in the end of the simulation), it was proposed the interpolation, classification and building of isoyetas precipitation maps, as shown in Figure 7.

The Figure 7(a) was built from the data observed in the 19 INMET automatic stations. Since the data are spatially unevenly distributed, it was adopted the Ordinary Kriging interpolation in order to estimate the precipitation in the places (pixels) without observed data. This technique is widely used when there are no values available for different parameters of interest in a given domain (not only precipitation), and it is the official technique used by the Brazil National Space Research Institute - INPE (acronym in Portuguese), in its website (INPE, 2014). Kriging is a geostatistical approach for surface estimation where the prediction at an unsampled location is calculated as a weighted linear combination of the available data that minimizes the expected squared error (VERDIN *et al*., 2016). It is important to say that the Kriging uses the observed data and irradiates

them to a certain distance that can be adjusted by the user. In case 7(a), it was used a 5 maximum search distance in SAGA Kriging algorithm (CONRAD, 2015).

The Figure 7(b) was built using the data obtained from the Giovanni Platform (https://giovanni.gsfc.nasa.gov/) product GPM_3IMERGHHL_v06, that is available hourly with a 0.1 degrees spatial grid, approximately 10 km. The data was integrated in time and space to the spatial and time discretization used in the watershed of interest, that is, the Paraiba do Sul River watershed. It was used an Ordinary Kriging as interpolation method in order to get a spatialization of precipitation (just like in the Figure 7a).

It must be pointed out that Figures 7(a-b) were used for visual comparison with the results obtained from WRF-ARM modelling and their values were not used to calculate the error metrics (Eqs. 1-4). The visual comparison between the interpolated maps from INMET automatic stations, Fig. 7(a), and the GPM estimates, Fig. 7(b), against the results from WRF was important.

The Figures 7(c-f) represent the results obtained with the WRF-ARW model for experiments 24, 41, 43 and 45, respectively. It was used an Ordinary Kriging as interpolation method in order to get a spatialization of precipitation (just like in the Figure 7a). In contrast Figure 7a, Figures 7(b-f) were generated from the points calculated by the model every ~ 5 km i.e. with a very large density of points.

Qualitative data analysis (visual) of Fig. 7(a-f) reveals that the group of best performing experiments with similar numerical results, as shown in Table 6, are not similar in spatialization distribution of precipitation. Even though Figures 7(d-f) have a similar spatialization of precipitation, Figure 7(c) presents a very different distribution. On can observe in Fig. 7(a-b) that the points where the accumulation of extreme rainfall is higher are not shown in the interpolated INMET automatic stations, Fig. 7(a), or the interpolated GPM data, such as Figs. 7(c-f), when they are compared with each other. So, in this is study, the researchers preferred to consider statistical metrics directly at the grid points locations where the meteorological stations are positioned.

Figure 7 – Accumulated Precipitation graphical representation for the Paraíba do Sul River Watershed
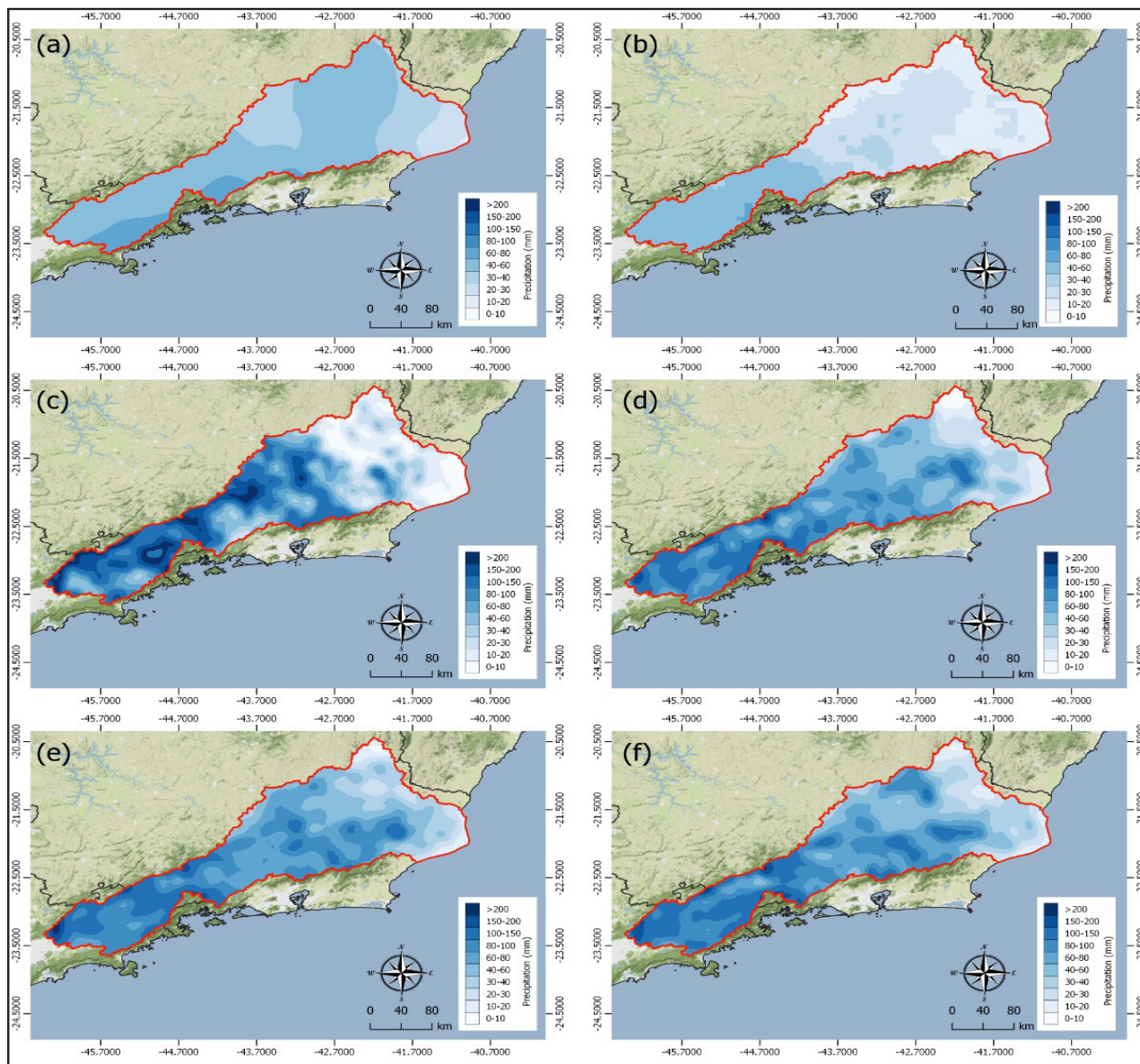
Source: Author's (2022)

(a) Observed data at INMET automatic stations with Ordinary Kriging interpolation. (b) Observed and modelled data from NOAA with Ordinary Kriging interpolation. (c) Predicted data from WRF model with experiment 24 and Ordinary Kriging interpolation. (d) Predicted data from WRF model with experiment 41 and Ordinary Kriging interpolation. (e) Predicted data from WRF model with experiment 43 and Ordinary Kriging interpolation. (f) Predicted data from WRF model with experiment 45 and Ordinary Kriging interpolation.

Table 8 – Results comparison for the best performing experiments (spatial cumulative analysis)

| Experiment	BIAS (mm)	MAE (mm)	RMSE (mm)
24	27.55	46.8	63.36
41	16.71*	22.76*	29.68*
43	21.13	25.2	32.71
45	21.37	25.91	33.43

Source: Author's (2022)

*Best results

The Table 8 shows the results of the calculated error metrics of BIAS, MAE and RMSE for the total cumulative rain, where the experiments 24, 41, 43 and 45 from the model, were compared with the values interpolated from the INMET stations. In this analysis (spatial) was possible to see that the experiments 41, 43 and 45 are numerically similar while experiment 24 is very different and presents the greater deviation (ratifying the visual analysis). As well as the mean analysis and the hourly mean analysis previously described, the spatial analysis presents experiment 41 with the smallest deviation, therefore, with the best performance.

The analysis of the linear correlation of the interpolated cumulative rainfall shows that experiments 41 and 45 stand out from the rest, with a R^2 result of 0.48 and 0.45 respectively, followed by experiment 43 with R^2 of 0.38 and the last position, the experiment 24 with large deviation with just 0.20 of R^2, as can be seen in Figure 8. These results confirm that experiment 41 is the best representative of the total precipitation into the watershed followed by experiment 45, and the experiment 24 is the worst, confirming the visual and metrics analyses. It is important to highlight that R^2 values found were low due the experiments have been tested in association with a small density of interpolated observed values, which does not represent consistently the rainfall into the large Paraiba do Sul watershed.

Figure 8 – Dispersion plot of the best performing simulations (spatial cumulative rainfall analyses)
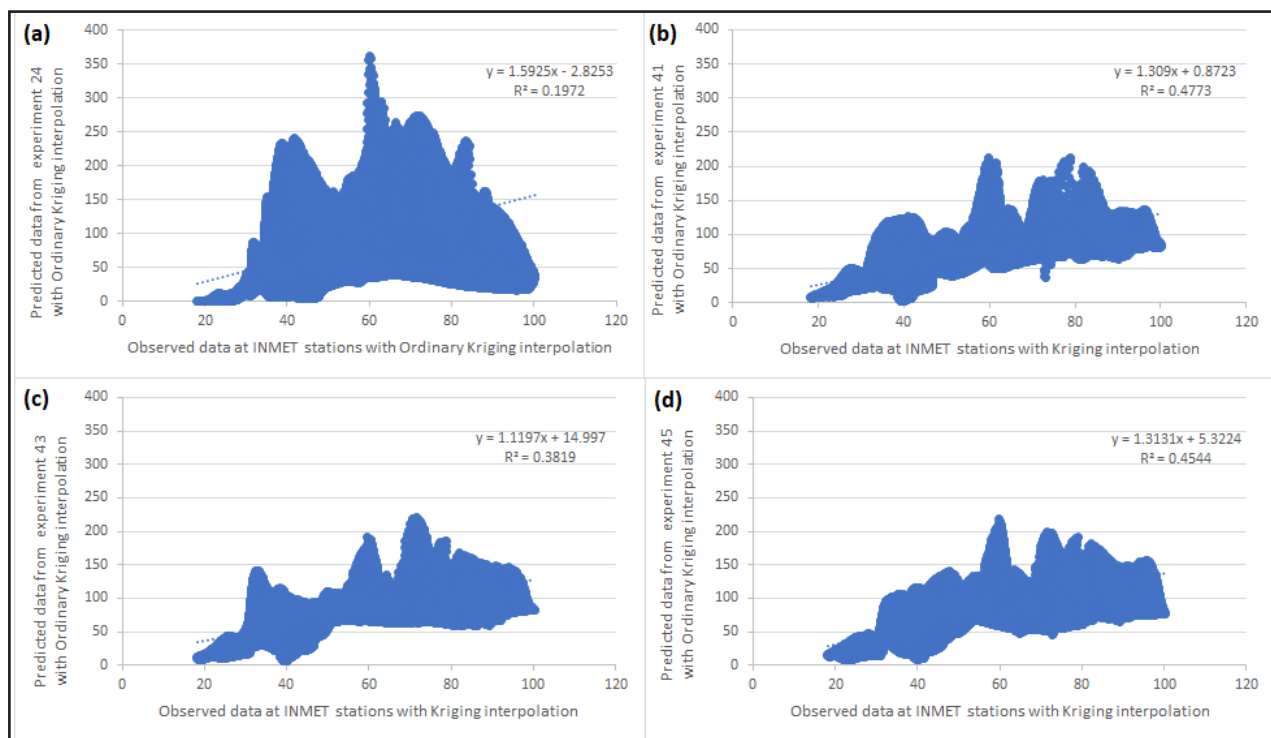
Source: Author's (2022)

(a) Linear correlation between cumulative rainfall from INMET stations with Ordinary Kriging interpolation and cumulative rainfall from experiment 24 with Ordinary Kriging interpolation. (b) Linear correlation between cumulative rainfall from INMET stations with Ordinary Kriging interpolation and cumulative rainfall from experiment 41 with Ordinary Kriging interpolation. (c) Linear correlation between cumulative rainfall from INMET stations with Ordinary Kriging interpolation and cumulative rainfall from experiment 43 with Ordinary Kriging interpolation. (d) Linear correlation between cumulative rainfall from INMET stations with Ordinary Kriging interpolation and cumulative rainfall from experiment 45 with Ordinary Kriging interpolation.

3 CONCLUSIONS

This study was conducted with the purpose of performing a sensitivity test to the physical parameters present in the WRF model, focusing on accumulated rainfall into the Paraíba do Sul River watershed.

For the planetary boundary layer, surface layer, land surface, longwave radiation and shortwave radiation, the Mellor-Yamada-Janjic, ETA model similarity theory, Noah

land surface model, RRTM and Dudhia schemes, respectively, were identified as the best performers. This result was obtained from tests performed in previous studies.

It was noticed, in this particular case, that the cumulus parameterization seems to be more important than microphysical scheme, and the best-performing was the Grell 3D convective scheme in all tested experiments.

The combinations of WSM5 and Grell-Freitas; Goddard and Grell 3D; Perdue Lin and Grell 3D; WSM5 and Grell 3D form a group with four numerically similar results. The experiments were subjected to a statistical analysis, with accumulated graphs interpretation, hourly graphs interpretation and spatial analysis from isoyetas. In general, they present similar results representing consistently the precipitation. The spatial analysis identified that experiment 24 differs from the others best-performing results. The ensembles of analyzes suggest that the combination of Goddard and Grell 3D might be considered as the one that best represented the average rainfall of the watershed, although the difference was not very significant.

Further investigation will be performed considering other periods of time. For forecast applications, this set of schemes can be used alone to provide different possibilities or can be ensembled together to provide one with smaller square mean error.

It is important to highlight that, the Paraíba do Sul River watershed has a great territorial extension, with a great latitudinal and altimetric variation, and therefore, the experiments aimed at finding an average representation of precipitation into the watershed. Thus, the effect caused at a point at which the model overestimates the observed data is counterbalanced by a point at which the model underestimates the observed data. So, a sensitivity testing in a single station or for another group of stations may present different results, being composed of a new sensitivity study to meet particular need.

ACKNOWLEDGEMENTS

REFERENCES

AVOLIO, E.; STEFANO, F. WRF simulations for a heavy rainfall event in southern Italy: Verification and sensitivity tests. **Atmospheric Research**, [*s.l.*], v. 209, p. 14-35, 2018.

BENDER, F. D. **Checking Sao Paulo weather forecast with WRF operating model.** 2012. 164p. Atmospheric Sciences Mastership Thesis – Instituto de Astronomia, Geofísica e Ciências Atmosféricas da Universidade de São Paulo: USP.

CALADO, R. N.; DERECZYNSKI, C. P.; CHOU, S. C.; SUEIRO, G.; MOURA, J. D. O.; RANDER, V.; BRASILIENSE, C. S. Eta-5km Model Simulation Performance Assessment for the Heavy Rainfall Case in the Paraíba do Sul River Basin in January 2000. **Revista brasileira de meteorologia**, [*s.l.*], v. 33, p. 83-96, 2018.

CEIVAP. **CEIVAP**. Geoenvironmental Data. Available in: www.ceivap.org.br/dados-gerais.php. Access on: Jun. 26th, 2019.

CHEN, S. H.; SUN, W. Y. A one-dimensional time dependent cloud model. **J. Meteor. Soc. Japan**, [*s.l.*], v. 80, p. 99–118, 2002.

COMIN, A.; JUSTINO, F.; PEZZI, L.; GURJÃO, C. D. S.; SHUMACHER, V.; FERNAÁNDEZ, A.; SUTIL. U. A. Extreme rainfall event in the Northeast coast of Brazil: a numerical sensitivity study. **Meteorology and Atmospheric Physics**, [*s.l.*], v. 133, p. 141–162, 2020.

CONRAD, O. **Module Simple Kriging. SAGA-GIS Module Library Documentation (v2.2.1).** 2015. Available in: http://www.saga-gis.org/saga_tool_doc/2.2.1/statistics_kriging_1.html. Access on Jun. 06th, 2020.

DI, Z.; DUAN, Q.; GONG, W.; WANG, C.; GAN, Y.; QUAN, J.; LI, J.; MIAO, C.; YE, A.; TONG, C. Assessing WRF model parameter sensitivity: A case study with 5-day summer precipitation forecasting in the Greater Beijing Area. **Geophysical Research Letters**, [*s.l.*], v. 42, n. 2, p. 579-587, 2015.

DUDHIA, J. Numerical study of convection observed during the winter monsoon experiment using a mesoscale two-dimensional model, J. **Atmos. Sci.**, [*s.l.*], v. 46, p. 3077–3107, 1989.

FERREIRA, P.; CASTANHEIRA, J. M.; ROCHA, A.; FERREIRA, J. Sensitivity study of surface forecasts in Portugal, by WRF, in view of the variation of physical parameters. *In*: Jornadas Científicas de la AME, 30, y el 9º Encuentro Hispano-Luso de Meteorología**. Acta de las Jornadas Científicas de la Asociación Meteorológica Española**. Zaragoza: Associación Meteorológica Española, 2008. Available in: https://pub.ame-web.org/index.php/JRD/article/view/2172. Access on Aug. 18th, 2022.

GRELL, G. A. Prognostic Evaluation of Assumptions Used by Cumulus Parameterizations. **Mon. Wea. Rev.**, [*s.l.*], v. 121, p. 764–787, 1993.

GRELL, G. A.; FREITAS, S. R. A scale and aerosol aware stochastic convective parameterization for weather and air quality modeling, Atmos. **Chem. Phys.**, [*s.l.*], v. 14, p. 5233-5250, 2014.

GRELL, G. A.; DEVENYI, D. A generalized approach to parameterizing convection combining ensemble and data assimilation techniques. **Geophys. Res. Lett.**, [*s.l.*], v. 29, 1693, 2002.

GUNWANI, P.; MOHAN, M. Sensitivity of WRF model estimates to various PBL parameterizations in different climatic zones over India. **Atmospheric research**, [*s.l.*], v. 194, p. 43-65, 2017.

HONG S. Y.; DUDHIA, J.; CHEN S. H. A revised approach to ice microphysical processes for the bulk parameterization of clouds and precipitation. **Mon Wea Rev**, [*s.l.*], v. 132, p. 103–120, 2004.

HONG, S-Y; LIM, J-O. J. The WRF single-moment 6-class microphysics scheme (WSM6). **Asia-Pacific Journal of Atmospheric Sciences**, [*s.l.*], v. 42, n. 2, p. 129-151, 2006.

INPE. **Information on monthly and seasonal climate monitoring products for rains in Brazil on the CPTEC / INPE.** Cachoeira Paulista: INPE, 2014. Available in: http://clima.cptec.inpe.br/~rclima1/pdf/Documento_produto_indice.pdf. Access on: May 25th, 2020.

JANJIC, Z. I. The Step–Mountain Eta Coordinate Model: Further developments of the convection, viscous sublayer, and turbulence closure schemes. **Mon. Wea. Rev.**, [*s.l.*], v. 122, p. 927–945, 1994.

KAIN, J. S. The Kain–Fritsch convective parameterization: An update. **J. Appl. Meteor.**, [*s.l.*], v. 43, p. 170–181, 2004.

KESSLER, E. On the Distribution and Continuity of Water Substance in Atmospheric Circulations. *In*: KESSLER, E. **On the Distribution and Continuity of Water Substance in Atmospheric Circulations.** Boston, MA: American Meteorological Society, 1969.

LIU, D.; YANG, B.; ZHANG, Y.; QIAN, Y.; HUANG, A.; ZHOU, Y.; ZHANG, L. Combined impacts of convection and microphysics parameterizations on the simulations of precipitation and cloud properties over Asia. **Atmospheric research**, [*s.l.*], v. 212, p. 172-185, 2018.

MAYOR, Y. G.; MESQUITA M. D. S. Numerical Simulations of the 1 May 2012 Deep Convection Event over Cuba: Sensitivity to Cumulus and Microphysical Schemes in a High-Resolution Model. **Advances in Meteorology**, [*s.l.*], v. 2015, e973151, p. 16, 2015.

MEYER, D.; RIECHERT, M. Open source QGIS toolkit for the Advanced Research WRF modelling system. **Environmental Modelling & Software**, [*s.l.*], v. 112, p. 166–178, 2019.

MOHAN, P. R.; SRINIVAS, C. V.; YESUBABU, V.; BASKARAN, R.; VENKATRAMAN, B. Simulation of a heavy rainfall event over Chennai in Southeast India using WRF: Sensitivity to microphysics parameterization. **Atmospheric Research**, [*s.l.*], v. 210, p. 83-99, 2018. https://doi.org/10.1016/j.atmosres. 2018.04.005.

PADILHA, S. F. Heavy rain event simulations in the state of Rio de Janeiro using the WRF model. 127p. Meteorology Mastership Thesis – Instituto de Geociências do Centro de Ciências Matemáticas e da Natureza: UERJ, 2011. PATEL, P., GHOSH, S., KAGINALKAR, A., ISLAM, S., & KARMAKAR, S. Performance evaluation of WRF for extreme flood forecasts in a coastal urban environment. **Atmospheric Research**, [*s.l.*], v. 223, p. 39-48, 2019.

QGIS. Web: http://www.qgis.org/en/site/forusers/download.html. Access in May 30th, 2019.

RODRÍGUEZ, L. G.; ANABOR, V.; PUHALES, F. S.; PIVA, E. D. Estimation of the probability of precipitation from nonparametric statistical techniques applied to numerical WRF simulations: a case study. **Ciência e Natura**, Santa Maria, v. 38, p. 491-497, 2016.

ROGERS, E.; BLACK, T.; FERRIER, B.; LIN, Y.; PARRISH, D.; DI MEGO, G. 2001. Changes to the NCEP Meso Eta Analysis and Forecast System: Increase in resolution, new cloud microphysics, modified precipitation assimilation, modified 3DVAR analysis. **NWS Technical Procedures Bulletin**, National Centers for Environmental Prediction NCEP. Maryland. Available in: https://www.emc.ncep.noaa.gov/mmb/mmbpll/mesoimpl/eta12tpb/. Access on Aug. 10th, 2022.

R-PROJECT. Index OF /SRC/BASE/R-3. Apache Server at cran.r-project.org Port 443. Disponível em: https://cran.r-project.org/src/base/R-3/. Access on Sept 10th, 2019.

SALES, D. S.; LUGON JUNIOR, J.; OLIVEIRA, V. P. S.; SILVA NETO, A. J. Rainfall input from WRF-ARW atmospheric model coupled with MOHID Land hydrological model for flow simulation in the Paraíba do Sul River. **Journal of Urban and Environmental Engineering (JUEE)**, v.15, n.2, p.188-203, 2021.

SILVA, F. P.; ROTUNNO FILHO, O. C.; SAMPAIO, R. G.; DRAGAUD, I. C. D. V; ARAÚJO, A. A. M.; SILVA, M. G. A. J; PIRES, J. D. Evaluation of atmospheric thermodynamics and dynamics during heavy-rainfall and no-rainfall events in the metropolitan area of Rio de Janeiro, Brazil. **Meteorology and Atmospheric Physics**, Springer-Verlag GmbH Áustria, v131, p. 299-311, 2019.

SILVA, F. P.; SILVA, M. G. A. J, MENEZES, W. F.; ALMEIDA, V. A. Evaluation of Atmospheric Indicators Using the WRF Numerical Model in Rain Events in Rio de Janeiro City. **Anuário do Instituto de Geociências**, v. 38, n. 2, p. 81-90, 2016.

SIMPSON, J.; KUMMEROW, C.; TAO W-K.; ADLER, R. F. On the tropical rainfall measuring mission (TRMM). **Meteorol Atmos Phys**, [*s.l.*], v. 60, p. 19–36, 1996.

SKAMAROCK, W.; KLEMP, J.; DUDHIA, J.; Gill, D.; BARKER, D.; DUDA, M.; HUANG, X.; WANG, W.; POWERS, J. 2019. A Description of the Advanced Research WRF Model Version 4. **NCAR Technical Note**, Colorado, NCAR/TN-556+STR, 145 p. Available in: doi:10.5065/1dfh-6p97.

Access on Sept 10th, 2019.

SOUZA, C. V. F.; RANGEL, R. H. O.; CATALDI, M. Numerical Assessment of the Influence of Urbanization on the Convection Regime and Precipitation Patterns of the São Paulo Metropolitan Region. **Revista Brasileira de Meteorologia**, [*s.l.*], v. 32, n. 4, p. 495-508, 2017.

TAO, W. K.; SIMPSON, J.; MCCUMBER, M. An ice-Water Saturation Adjustment. **Monthly Weather Reviews**, [*s.l.*], v. 117, p. 231–235, 1989.

TIEDTKE, M. A comprehensive mass flux scheme for cumulus parameterization in large–scale models. **Mon. Wea. Rev.**, [*s.l.*], v. 117, p. 1779–1800, 1989.

VERDIN, A.; FUNK, C.; RAJAGOPALAN, B.; KLEIBER, W. Kriging and Local Polynomial Methods for Blending Satellite-Derived and Gauge Precipitation Estimates to Support Hydrologic Early Warning Systems. **IEEE Transactions on Geoscience and Remote Sensing**, v. 54, n. 5, p. 2552-2562, 2016. DOI: 10.1109/TGRS.2015.2502956.

WANG, W.; BRUYERE, C.; DUDA, M.; DUDHIA, J.; GILL, D.; LIN, H. C.; MICHALAKES, J.; RIZVI, S.; ZHANG, X.; BEEZLEY, J. D.; COEN, J. L.; KAVULICH, M.; WERNER, K.; CHEN, M.; BERNER, J.; MUNOZ-ESPARZA, D.; REEN, B.; FOSSEL, K.; MANDEL, J. ARW Version 4 Modeling System User's Guide. **NCAR Technical Note**, Colorado. 2019. Available in: https://pdfcoffee.com/version-4-modeling-system-users-guide-january-2019-pdf-free.html. Access on Aug. 18th, 2022.

WARNER, T. T. **Numerical weather and climate prediction.** Cambridge University Press, 2010.

WRF Modeling System Download. WRF USERS PAGE, c2017. WRF Source codes and graphics software downloads. Available: http://www2.mmm.ucar.edu/wrf/users/download/get_source.html. Access on Sept. 14th, 2019.

YANG, Q.; DAI, Q.; HAN, D.; CHEN, Y.; ZHANGA, S. Sensitivity analysis of raindrop size distribution parameterizations in WRF rainfall simulation. **Atmospheric Research**, [*s.l.*], v. 228, p. 1-13, 2019. https://doi.org/10.1016/j.atmosres.2019.05.019.

ZHANG, C.; WANG, Y. and HAMILTON, K. Improved representation of boundary layer clouds over the southeast pacific in ARW–WRF using a modified Tiedtke cumulus parameterization scheme. **Mon. Wea. Rev.**, [*s.l.*], v. 139, p. 3489–3513, 2011.

ZHANG, C.; WANG, Y. Futuras Mudanças Projetadas da Atividade de Ciclones Tropicais sobre o Norte do Norte e Pacífico Sul em um Modelo Climático Regional de 20 km de Malha. **J. Climate**, [*s.l.*], v. 30, p. 5923-5941, 2017.

Authorship contributions

1 – Dhiego da Silva Sales

Geographer, M.Sc. in Environmental Engineering

https://orcid.org/ 0000-0001-6541-4720 • dhiego.sales@outlook.com

Contribution: Conceptualization | Data curation | Investigation | Methodology | Writing original draft |Software | Validation | Visualization

2 – Jader Lugon Junior

Mechanical Engineer, D.Sc. in Computational Modeling

https://orcid.org/0000-0001-8030-0713 • jlugonjr@gmail.com

Contribution: Conceptualization | Methodology | Software | Supervision | Validation | Visualization

3 – Vicente de Paulo Santos de Oliveira

Surveying Engineer, D.Sc. in Agricultural Engineering

https://orcid.org/0000-0002-5981-0345 • vicentepsoliveira@gmail.com

Contribution: Conceptualization | Methodology | Supervision | Validation | Visualization

4 – Nivaldo Silveira Ferreira

Meteorologist, D.Sc. in Meteorology

https://orcid.org/ 0000-0001-7427-3958 • nivaldosf@uenf.br

Contribution: Conceptualization | Methodology | Visualization

5 – Antonio José Silva Neto

Mechanical Engineer, D.Sc. in Mechanical Engineer

https://orcid.org/0000-0002-9616-6093 • ajs_neto@uol.com.br

Contribution: Conceptualization | Methodology | Visualization

How to quote this article